Studies and optimization of Pohang Light Source-II superconducting radio frequency system at stable top-up operation with beam current of 400 mA

Youngdo Joo,[a] Inha Yu, Insoo Park, Myunghwan Chun, Byung-Joon Lee, Ilmoon Hwang, Taekyun Ha, Seunghwan Shin, and Younguk Sohn
Pohang Accelerator Laboratory, Pohang University of Science and Technology, Pohang 790-784, Korea

(Received 14 October 2014; accepted 3 December 2014; published online 15 December 2014)

After three years of upgrading work, the Pohang Light Source-II (PLS-II) is now successfully operating. The final quantitative goal of PLS-II is a top-up user-service operation with beam current of 400 mA to be completed by the end of 2014. During the beam store test up to 400 mA in the storage ring (SR), it was observed that the vacuum pressure around the radio frequency (RF) window of the superconducting cavity rapidly increases over the interlock level limiting the availability of the maximum beam current storing. Although available beam current is enhanced by setting a higher RF accelerating voltage, it is better to keep the RF accelerating voltage as low as possible in the long time top-up operation. We investigated the cause of the window vacuum pressure increment by studying the changes in the electric field distribution at the superconducting cavity and waveguide according to the beam current. In our simulation, an equivalent physical modeling was developed using a finite-difference time-domain code. The simulation revealed that the electric field amplitude at the RF window is exponentially increased as the beam current increases, thus this high electric field amplitude causes a RF breakdown at the RF window, which comes with the rapid increase of window vacuum pressure. The RF accelerating voltage of PLS-II RF system was set to 4.95 MV, which was estimated using the maximum available beam current that works as a function of RF voltage, and the top-up operation test with the beam current of 400 mA was successfully carried out. © *2014 AIP Publishing LLC*. [http://dx.doi.org/10.1063/1.4904188]

I. INTRODUCTION

Synchrotrons were originally used exclusively in the field of particle physics, allowing scientists to study collisions between subatomic particles with higher and higher energies. However, when high-energy electrons are forced to travel in a circular orbit, they release extremely intense radiation. This radiation was called synchrotron light since it was observed for the first time in a synchrotron. Due to the usefulness of synchrotron light, many accelerators today now exist solely to generate light for scientific experiments. Facilities dedicated to the production and use of synchrotron light are known as a synchrotron light source.

First-generation synchrotron light sources were basically beamlines built onto existing facilities designed for particle physics studies. Second-generation synchrotron light sources were dedicated to the production of synchrotron radiation and employed electron storage rings (SRs) to harness the synchrotron light. Current (third-generation) synchrotron light sources optimize the intensity of the light by incorporating long straight sections into the storage ring for "insertion devices" (IDs) such as undulator and wiggler magnets. Wigglers create a broad but intense beam of incoherent light. Undulators create a narrower and significantly more intense beam of coherent light, with selected wavelengths, or "harmonics," which can be "tuned" by manipulating the magnetic field in the device.

The unique properties of synchrotron light, such as a continuous spectrum extending up to X-ray region from vacuum ultraviolet, great intensity, and a high degree of polarization, as well as the possibility of exact theoretical verification have resulted in extensive theoretical and technical application of synchrotron light. This synchrotron light have opened up vast and new prospects of the investigation in experiments with polarized beams of particles in high energy physics, in the solid state physics (photoelectron spectroscopy, crystallography, X-ray luminescence, etc), chemistry, biology (study of DNA molecule structure), medicine, geology (elemental analysis), ecology (analysis of atmospheric aerosols, soil, and water), and creates new advanced technologies (microelectronics, micromechanics, constructing new composite materials), etc.

The Pohang Light Source (PLS) of the Pohang Accelerator Laboratory (PAL), one of the third-generation of synchrotron light sources, has been making a significant contribution to scientific research during the 14 years of its successful operation. In March 2009, the PAL upgraded the PLS, and the PLS-II upgrade was completed to meet the increasing demand from the growing user community. The PLS-II upgrade has increased the beam energy from 2.5 GeV to 3 GeV; the number of IDs has been increased by a factor of two (20 IDs); and the beam current has been increased from 190 mA to 400 mA. The beam emittance has been reduced to below 10 nm while retaining the existing PLS tunnel as well as the existing injection system.[1,2]

The radio-frequency (RF) system of the electron SR for the light source generates a sufficient RF accelerating voltage and transfers RF power to the electron beam to compensate for the beam energy loss due to synchrotron radiation

[a]Author to whom correspondence should be addressed. Electronic mail: Ydjoo77@postech.ac.kr.

from the bending magnets and IDs. Three superconducting RF systems are installed in the PLS-II storage ring, in contrast to the five normal conducting RF systems that had been installed in the PLS storage ring.[3,4]

The schematic drawing of RF system in PLS-II storage ring is shown in Fig. 1(a). The PLS-II RF system consists of four major components: (1) a continuous wave (CW) klystron with a rated output power of 300 kW at the frequency of about 500 MHz, (2) a 300 kW circulator which isolates the klystron to protect the klystron form reflection power from cavity, (3) a 300 kW water cooling ferrite load which terminates the RF power by converting the RF power to thermal loss at the ferrite panel, and (4) a CESR-B type cryomodule produced by RI (former ACCEL). The cut-view of the cryomodule is shown in Fig. 1(b). A single-cell Niobium (Nb) cavity is sunk into the liquid helium contained in a He vessel and is preserved at superconducting state. Three cold cathode gauges are installed at the cavity upstream taper section, the cavity downstream taper section and the window pumping out port to measure the vacuum pressure of the upstream vacuum, downstream vacuum, and window vacuum, respectively.

The RF power generated by klystron is incident to the superconducting cavity (SC) through WR1800 waveguide, the ceramic RF vacuum window and the RF coupler to build a RF field at the SC RF cavity. The low level RF (LLRF) system gets the amplitude and phase information of the RF field from the signal at the cavity RF pickup and keeps the RF field stable by controlling the amplitude and phase of forward power in the presence of various external noises such as beam loading effect, mechanical vibrations, changes in the electrical length of the waveguide between the klystron and the cavity, and the pressure fluctuation in the LHe vessel.

An RF accelerating voltage is the maximum energy which an electron can obtain from the RF field when the electron goes through the cavity on phase. The PLS-II RF system has three SCs (SC1, SC2, and SC3) and each cavity phase is adjusted in-phase, which means that the electron enters each cavity at the same phase of cavity field. Therefore, the total RF accelerating voltage of SR coincides with the linear summation of the RF accelerating voltages of three SCs.

Figure 2(a) shows the changes in the energy acceptance and the Touschek lifetime[5] that are caused by the RF accelerating voltage of PLS-II SR. As the RF accelerating voltage increases, the energy acceptance increases, as a result, the injection efficiency becomes higher. However, the energy acceptance of 2.5% is already sufficient for the injection efficiency of the PLS-II SR. Therefore, the effect of the RF accelerating voltage higher than 3.6 MV on the injection efficiency is saturated. The Touschek lifetime keeps increasing until the RF accelerating voltage reaches about 3.6 MV, but it gets lower for the RF accelerating voltage higher than 3.6 MV. The longitudinal bunch length becomes shorter as the RF accelerating voltage increases as shown in Fig. 2(b). The shorter bunch can cause the problem of ion instability due to

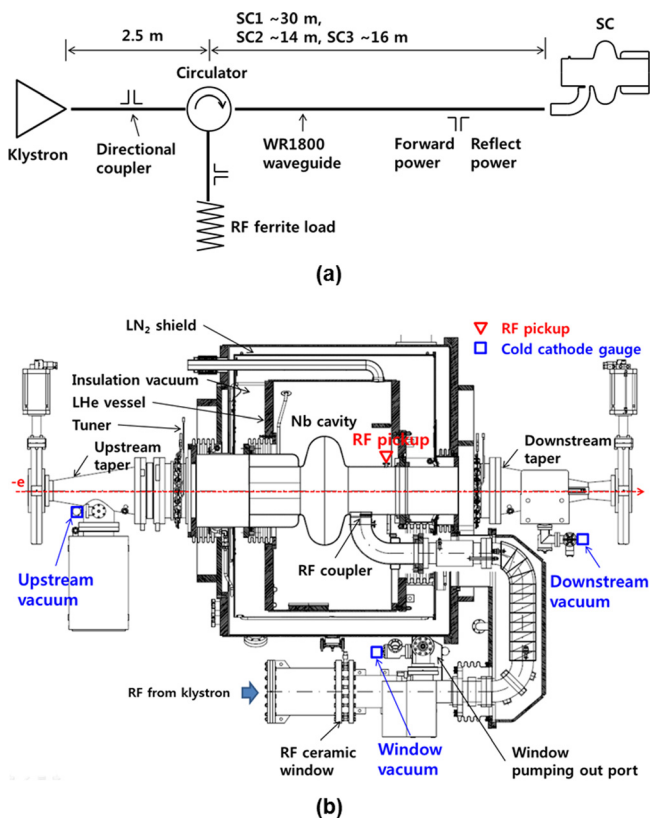

FIG. 1. (a) Schematic diagram of the superconducting RF system in the PLS-II storage ring and (b) the cut-view of the CESR-B type Cryomodule.

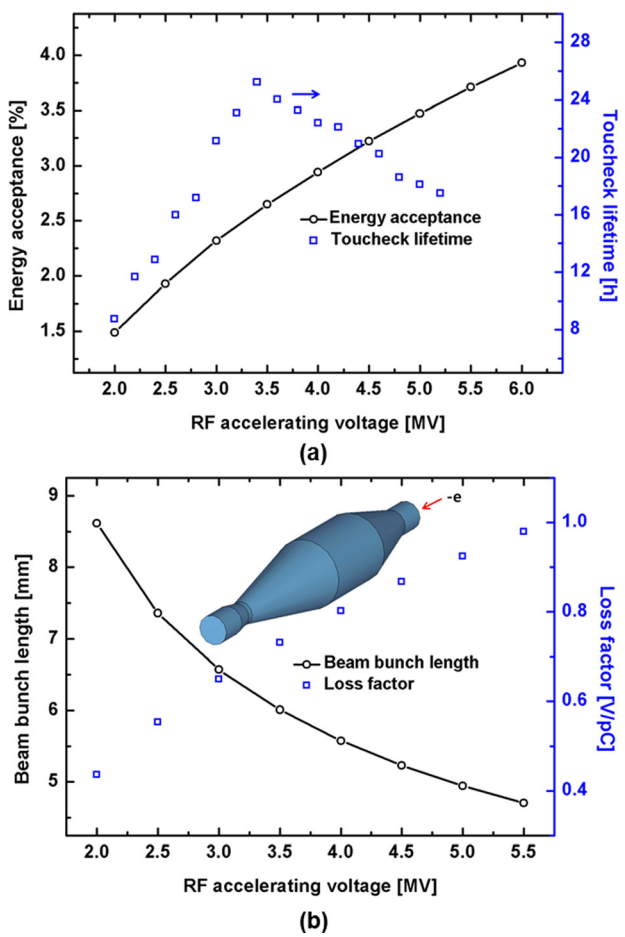

FIG. 2. (a) Calculated energy acceptance and Touschek lifetime and (b) the beam bunch length and the loss factor of the PLS-II SC taper section. The three-dimensional modeling of the SC taper section is shown in the inset.

the short bunch interacting more strongly with the impedance of the vacuum chamber, enhancing outgassing in some local points. For an instance, the loss factor of the SC cavity taper section in the PLS-II SR is calculated and shown in Fig. 2(b). When the RF accelerating voltage increases from 3.6 MV to 5.0 MV, the beam bunch length is reduced by 17.5% and the loss factor is enlarged by 26.4%. This enlarged loss factor means that more power loss due to the wake-field occurs at the taper section increasing the surface temperature and vacuum pressure.

Also from the SC RF cavity operational point of view, operating a SC at a higher RF accelerating voltage is restrictive to long stable operation since it increases the possibility of cavity quench as well as rapid vacuum pressure increase. Moreover, as the RF accelerating voltage grows, the ohmic quality factor (Q_o) decreases. Consequently, the cryogenic load increases even though the maximum available RF accelerating voltage of the PLS-II SC as high as 2.2 MV per a cavity. Therefore, it is recommended that the total RF accelerating voltage be kept at around 3.6 MV.

At the beam store test conducted with the RF accelerating voltage of 3.6 MV, the RF accelerating voltage of each of the three SCs was equally set to 1.2 MV. Figure 3(a) shows the measured beam current, the forward and reflect powers and vacuum pressures of SC2 during the beam store test. At the stand-by state with no beam presence, the forward power incident to SC and the reflect power from SC are almost the same because there occurs total reflection at the SC and the dissipated loss at SC wall is as low as below 10 W. As the stored beam current increases, the beam power gets larger, which the electron beam gets from the cavity field, and the LLRF system enhances the forward power to maintain the RF accelerating voltage in the SC. Therefore, the forward power increases during the beam injection while the reflection power decreases. The vacuum pressure of upstream and downstream of the SC has a current dependency because the outgassing from photon mask located near the SC comes into the SC while the vacuum pressure at the window is relatively stable. When the beam current come to about 235 mA, the forward power and reflect power of SC2 are getting unstable. Then, the vacuum pressure at the window of SC2 is sharply increased to the interlock level at the beam current of about 259 mA so that the interlock system turn off the RF system and the beam current is dumped. The other RF systems of SC1 and SC3 are also down because LLRF system cannot hold the control in the rapid beam dump case. It is noted that only the window vacuum is sharply increased in a short time.

In the second beam store test, the RF accelerating voltage of each cavity was set to 1.3 MV. Fig. 3(b) shows the measured beam current, the forward and reflect powers, and vacuum pressures of SC2 during the second beam store test. The unstable forward and reflect power are observed from the beam current of 283 mA, and the beam current is dumped by the window vacuum pressure interlock of SC2 at the beam current of 312 mA. When the results of the two beam store tests are compared, we can see the same event-set but only the beam current at which the event arises is increased

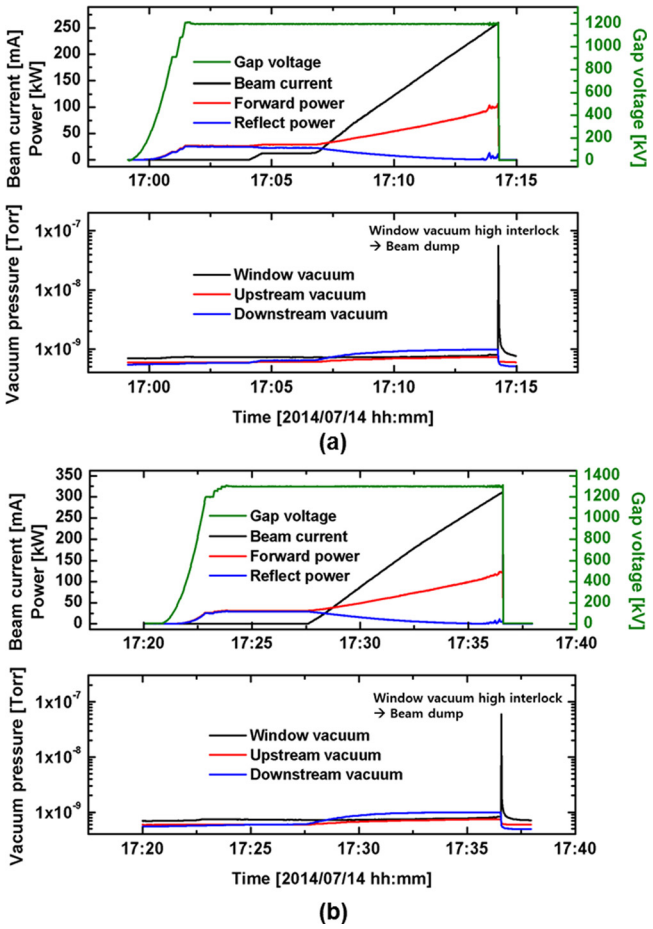

FIG. 3. The beam current, forward power, and reflect power measured and the vacuum pressures of SC2 during the beam store test with the RF accelerating voltage of (a) 1.2 MV and (b) 1.3 MV.

about 50 mA. It can be deduced that the maximum available beam current is limited by the RF accelerating voltage.

This paper examines what causes the window vacuum of SC2 to increase sharply when the reflect power is near zero during the beam storing test and then analyzes the relation between the RF accelerating voltage and the beam current. Based on the result, we estimate the optimized RF accelerating voltage for 400 mA in PLS-II SR.

II. ESTIMATED CHANGE OF RF POWERS TO THE BEAM CURRENT

When the RF accelerating voltage (V_c) is applied to the RF cavity, the required forward power (P_f) for given beam current (I_b) is

$$P_f = \frac{[(1+\beta)P_c + P_b]^2}{4\beta P_c}, \tag{1}$$

where $P_c = \frac{V_c^2}{(R/Q)Q_o}$ (dissipated power at the cavity surface), $P_b = V_{loss/turn} I_b$ (beam power), $\beta = \frac{Q_o}{Q_e}$ (coupling ratio), and $V_{loss/turn}$ is the energy loss per turn in the unit of eV.

The energy losses per turn by radiation in bending magnet and IDs are 1042 keV and 200 keV, respectively. The R/Q and the ohmic quality factor (Q_o) of CESR-B type

SC are 89 ohm and about 1.1e9, respectively. The measured external Q (Q_e) of SC1, SC2, and SC3 are 1.62×10^5, 1.65×10^5, and 1.52×10^5, respectively.

The measured forward power, reflect power, and window vacuum pressure from Fig. 3(a) are reproduced to the beam current domain and shown in Fig. 4(a) together with the calculated beam power, forward power and reflect power of SC2 with the RF accelerating voltage of 1.2 MV. The calculated and measured powers are well matched until the beam current reaches 235 mA. However, the measured powers become unstable and show difference from calculated powers when the current is higher than 235 mA. Both the forward power and the reflect power are larger than those calculated. That means that the coupling ratio of the cavity is changed. When the beam current is dumped, it reaches 259 mA due to the window vacuum high interlock. The measured powers with the RF accelerating voltage of 1.3 MV are also compared with the calculated powers in Fig. 4(b). One can see exactly the same phenomena as those shown in Fig. 4(a) except that the beam current where the RF powers start to show unstable behavior is increased to 283 mA and beam dump current is increased to 312 mA.

The unpredictable changes in the coupling ratio and the rapid increment of window vacuum pressure strongly suggest that the changes in the electric field distribution must be examined at and around the ceramic window in the beam current domain.

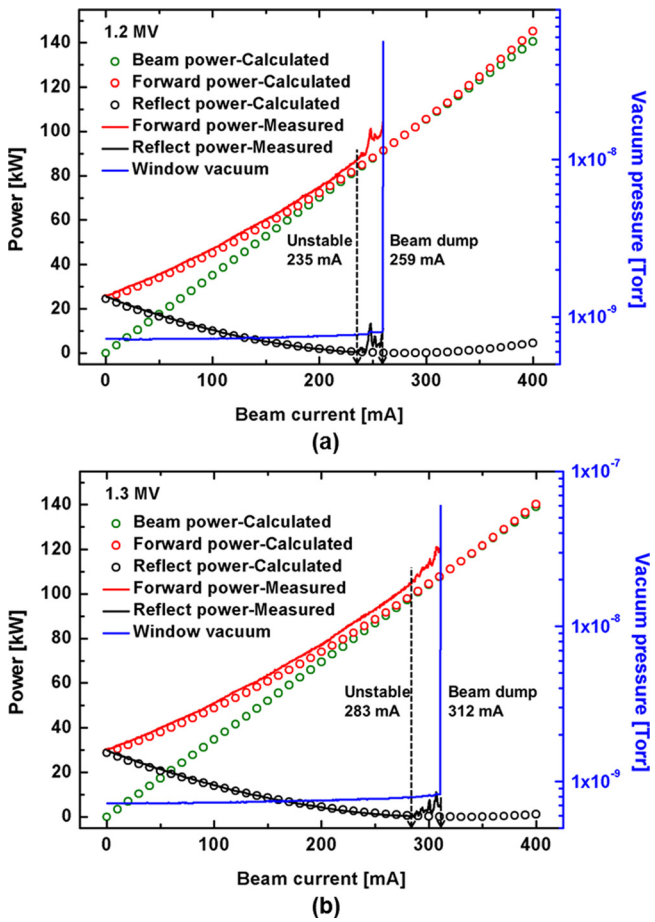

FIG. 4. The beam power, forward power, and reflect power calculated, and the forward power, reflect power measured, and the window vacuum pressure of SC2 in the beam current domain during the beam store test with the RF accelerating voltage of (a) 1.2 MV and (b) 1.3 MV.

III. ELECTRIC FIELD DISTRIBUTION AT CERAMIC WINDOW

The electric field distribution is simulated using a full three-dimensional finite-difference time-domain (FDTD) simulation code, CST Particle Studio.[6] The simulation model is shown in Fig. 5. The klystron forward power is represented as an input power through the Port 1. It is noted that a virtual external coupling structure with a waveguide port (Port 2) is made at the downstream of SC to represent the beam power which the electron beam takes from the cavity RF accelerating field. As the length of the external coupling structure (Coupler_l) gets longer, the coupled out power through Port 2 gets larger, and this means that in this equivalent physical modeling, the beam power and the beam current are larger.

To directly compare the electric field amplitude at the cavity and waveguide in the case of different Coupler_l, the field calculation line is set as drawn in Fig. 5. Then, the electric field amplitude along the line is simulated and plotted in Fig. 6(a). Here, the electric field amplitude for each Coupler_l is normalized to the maximum value at the cavity center, because the LLRF system controls the cavity RF accelerating field to be fixed despite the changes in the beam power and beam current. The magnified view of the dotted-box region is shown in Fig. 6(b). The SC acts like a wall, so the resonance field is built up in the waveguide region. The RF window is located at the position of minimum electric field when Coupler_l is short. That means the window is located at the anti-node of resonance field with no beam current presence. This is a common RF circuit design criterion. However, as Coupler_l is longer, the phase of resonance field is changed to invert so that the window is now located at maximum electric field amplitude. In addition, the maximum electric field amplitude of the resonance gets higher as Coupler_l increases because the forward power should be increased to maintain the cavity RF field. That means that the electric field amplitude at the RF window gets higher as the beam current increases.

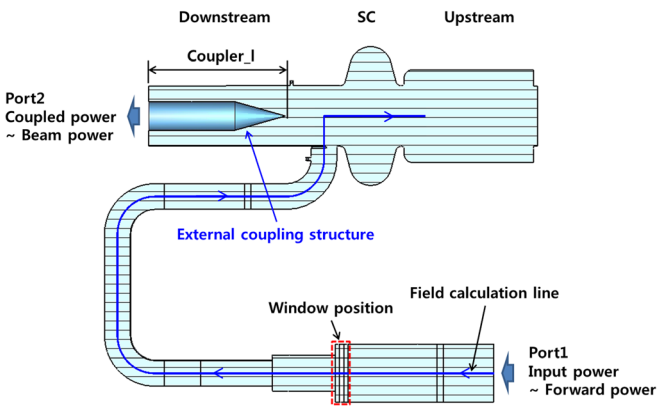

FIG. 5. The simulation model of the CST Particle Studio.

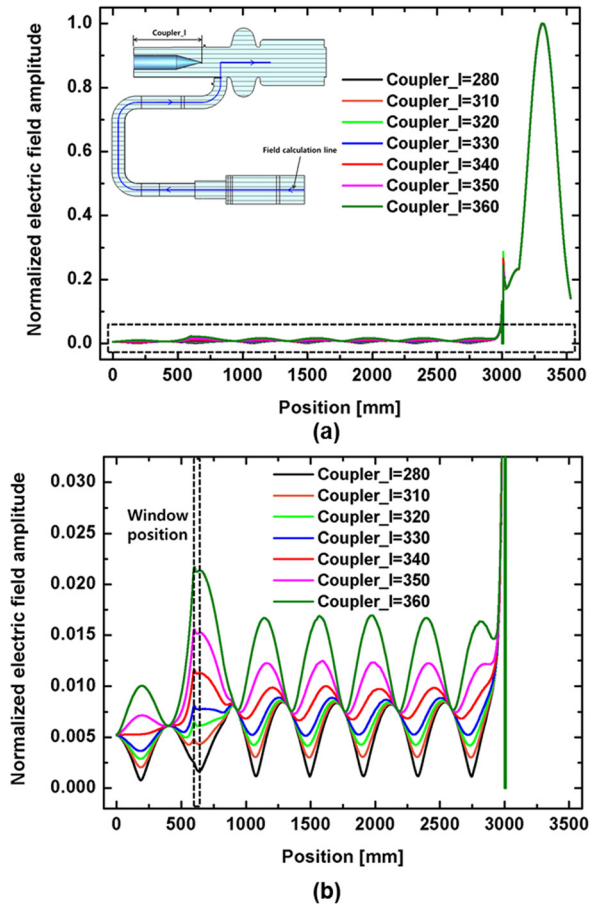

FIG. 6. (a) Changes that occurred in the simulated normalized electric field amplitude due to Coupler_l and (b) the magnified graph of the dotted-box region shown.

In order to see examine the changes in the electric field amplitude at the RF window to Coupler_l, the electric field amplitude at the RF window is re-normalized to that of the case where Coupler_l is zero and plotted in Fig. 7. The forward power (P_f) and reflect power (P_r) at the Port 1 are simulated with the change of Coupler_l and the power ratio (P_r/P_f) is also plotted as a function of Coupler_l in Fig. 7. At first, the power ratio is almost 1 when Coupler_l is zero. This means there occurs total reflection in the waveguide because the cavity-waveguide is highly over-coupled with no beam presence. As Coupler_l is getting longer, the power ratio is reduced and the electric field at the RF window starts to exponentially increase. The power ratio becomes zero when Coupler_l is around 340 mm, which means that the cavity-waveguide is critical-coupled. At this time, the electric field amplitude at the RF window is about five times higher than that of no beam presence. The power ratio turns to increase for Coupler_l longer than 340 mm, and now the cavity-waveguide is under-coupled. It can be summarized that the appearance of electron beam in very high-Q cavity causes change in cavity coupling ratio and, as a consequence, change in field distribution at the RF window.

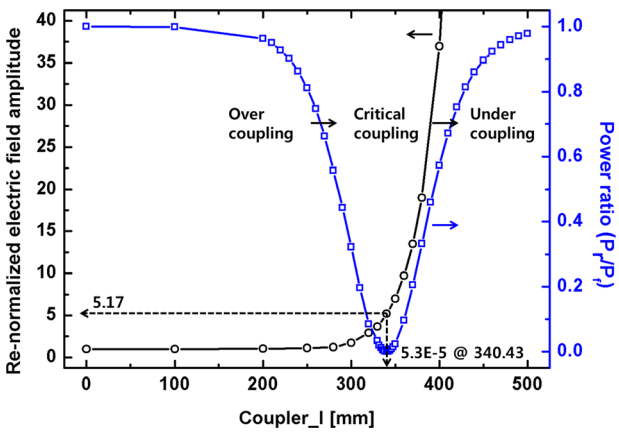

FIG. 7. Changes in the re-normalized electric field amplitude at the RF window position that are caused by Coupler 1 and changes in the power ratio of the reflect power-to-forward power that are caused by Coupler 1.

It is also noted that the resonance frequency of the operating mode in the cavity is shifted with the electron beam presence due to the reactive part of full impedance. When Coupler_l is changed from 0 mm to 340 mm in the simulation, the resonance frequency is shifted by about 6 kHz. This resonance frequency shift caused by the appearance of electron beam can be also measured from the frequency tuner displacement. The tuner displacement compensating the resonance frequency shift is measured about 0.4 mm during the beam storing test up to 400 mA and this tuner displacement is equal to the frequency shift of about 7 kHz. Both simulation and measurement show similar value which is small compared to the operation frequency of 500 MHz, and therefore, the influence of the reactive part of full impedance on power balance in cavity can be negligible.

IV. DISCUSSION ON THE ELECTRIC FIELD AMPLITUDE AT THE RF WINDOW

The RF ceramic window which allows an RF power matching between air and ultra-high vacuum parts is made of alumina with a thin Ti/N coating. The thin film suppresses the multipactor effect on RF alumina surface due to its low secondary electron emission yield.[7,8] Nevertheless, the RF window has more chance of RF breakdown which is caused by the multipactor effect (electron multiplication on the surface) and/or the discharge of accumulated charges that occurs when the RF window is exposed to a higher electric field. As the beam current increases, the electric amplitude at the RF window exponentially grows as shown in Fig. 7. Even though a well-conditioned RF window withstands at higher electric field than a newly installed RF window does, the RF breakdown with the increasing of vacuum pressure is inevitable. In addition, the standing wave ratio of the RF window can be varied in the early stage of RF breakdown due to the multipactor effect and, therefore, the forward power and reflect power becomes unstable.[9] The maximum available beam current is limited to the beam current where the unstable behavior of the forward power and reflect power occurs.

The data set of Figs. 3(a) and 3(b) is reproduced to compare the changes in power ratio to the beam current in the cases of the RF accelerating voltage of 1.2 MV and 1.3 MV as shown in Fig. 8. In both cases of 1.2 MV and 1.3 MV,

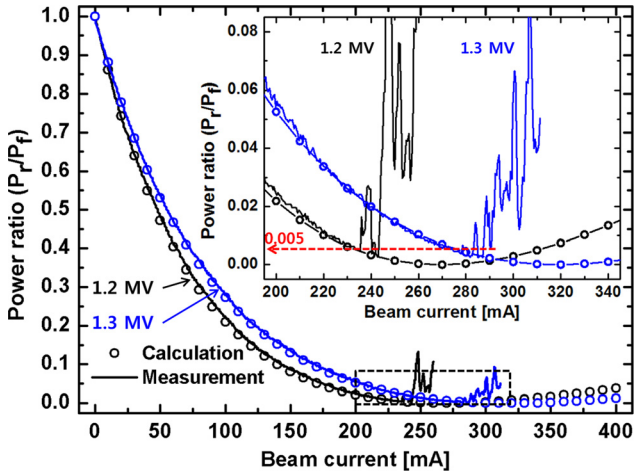

FIG. 8. Changes in the calculated power ratio and the measured power ration caused by the beam current. The dotted-box area is enlarged and shown in the inset.

the measured power ratio (solid line) deviates from the calculated power ratio (circles), and it becomes unstable when the power ratio comes to about 0.005. As shown in Fig. 7, the electric field amplitude at RF window for the power ratio of 0.005 is about five times the power ratio of 1 (no beam presence). At early stage where the RF window is installed a new, the RF window cannot withstand such high electric field amplitude since it is not sufficiently conditioned, and, therefore, RF breakdown occurs at a higher power ratio. In other words, the maximum available beam current becomes low even at the same RF accelerating voltage while the new RF window is not yet fully conditioned. The RF window of the PLS-II is already well-conditioned through the continuous operation for more than a year, so it can withstand this electric field amplitude. The power ratio for the maximum available beam current for PLS-II SC is 0.005 (near zero), and the maximum available beam current may be estimated from the beam current for zero power ratio.

The reflect power (P_r) is given as a simple equation of the forward power (P_f), cavity dissipate power (P_c), and beam power (P_b) when the other RF power loss is ignored, so that

$$P_r = P_f - P_c - P_b = 0. \tag{2}$$

The beam current ($I_{b,o}$) for zero power ratio is easily calculated from (1) and (2)

$$I_{b,o} = \frac{(\beta - 1)P_c}{V_{loss/turn}} = \frac{\frac{Q_o}{Q_e} - 1}{V_{loss/turn}} \cdot \frac{{V_c}^2}{\left(\frac{R}{Q}\right)Q_o}. \tag{3}$$

Here, $V_{loss/turn}$ is fixed by the PLS-II SR. The R/Q and Q_o are also determined by the cavity production. Equation (3) tells that $I_{b,o}$ is proportional to the square of RF accelerating voltage and $I_{b,o}$ is inversely proportional to Q_e. Therefore, the stable operation beam current can be increased by increasing the RF accelerating voltage of SC. In addition, SC2 faces the RF window breakdown earlier than other SCs, because it has the highest Q_e among three SCs.

V. RF ACCELERATING VOLTAGE FOR 400 mA TOP-UP OPERATION

The $I_{b,o}$ for the cavity RF voltage of 1.2 MV and 1.3 MV are calculated as 235 mA and 283 mA, respectively, and therefore, the differences from the measured maximum available current are only 34 mA and 36 mA, respectively. Now, one can estimate the required RF accelerating voltage for the 400 mA beam current operation.

The top-up operation test with the beam current of 400 mA is carried out. The measured data set is shown in Fig. 9. During the test, the gap distance of IDs is set to the value of normal user service, and the total energy loss is about 1242 keV/turn (energy losses by radiation in bending magnets and IDs are 1042 keV/turn and 200 keV/turn, respectively).

At first, the RF accelerating voltages of each SC are equally set to 1.6 MV as shown in the region A in Fig. 9. The SC2 RF accelerating voltage is controlled at slightly lower than the setting value because the LLRF output power limit is set to wrong value by mistake. Nevertheless, the stable top-up operation with beam current of 400 mA beam is observed. The beam current slip from 400 mA is caused by the klystron-modulator fault of the linear accelerator (LINAC), which injects 3 GeV electrons to the PLS-II SR. The vacuum pressure of the SR vacuum chamber is higher than that of normal state because it is first time to operate the SR in 400 mA top-up operation. The high vacuum pressure reduces the beam lifetime, consequently, the injection interval should be changed (from 180 to 120 seconds) to maintain 400 mA top-up operation.

However, no significant problem on the RF system is observed, even though the fluctuation of the amplitude and phase of the RF field is higher than the operation limit because of the rough setting of LLRF control parameters. The reflect power of SC2 is measured to be around 1–3 kW. In order to secure the operation margin and to reduce the chance of RF breakdown in the electric field at the RF window for a stable long time user-service operation, the RF accelerating voltages of each SC are equally set to 1.65 MV as shown in the region B in Fig. 9. At this time, the LLRF power limit is set to right value and all the RF accelerating

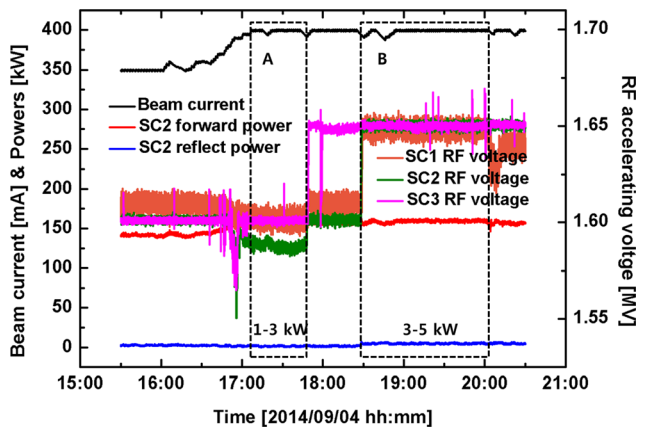

FIG. 9. The beam current, RF voltages, forward power, and reflect power measured during the top-up operation test with the beam current of 400 mA.

voltages are controlled at 1.65 MV. The reflection power is now increased to around 3–5 kW. The 400 mA top-up operation test was carried out for more than three hours without any fault.

VI. SUMMARY AND FUTURE WORKS

We studied the effect of beam current on the electric field distribution at the SC-waveguide by simulating an equivalent physical modeling, which represents beam power as an external coupling structure and waveguide port. The RF window is located at the minimum peak of the electric field distribution when no beam is presented. The phase of electric field distribution at the SC-waveguide is changed to invert as the beam current increases, and, therefore, the RF window is located at maximum peak of the electric field distribution. Moreover, the LLRF system puts more klystron forward power into the SC to maintain the cavity accelerating field as the beam current increases, and, therefore, the electric field amplitude at the RF window is exponentially increased. This high electric field amplitude raises the probability of RF breakdown of the RF window, which comes with a rapid increase of the window vacuum pressure. The maximum available beam current is estimated as a function of the RF accelerating voltage. Based on this estimation, we set the total RF accelerating voltage to 4.95 MV and successfully carried out the top-up operation test with the beam current of 400 mA. Even though the Touschek lifetime is reduced to about 18 hours for the operating RF accelerating voltage of 4.95 MV, we confirmed that no significant problem occurs in the stable 400 mA top-up operation.

To the best of our knowledge, this is the first quantitative study conducted on the effect of beam current on electric field distribution at the RF window. Now the efforts to reduce the RF accelerating voltage to 3.6 MV are underway. For instance, an experimental test will be conducted to reduce the Q_e of the cavity-waveguide using a stub tuner.

ACKNOWLEDGMENTS

The authors thank Dr. S. Pande (DIAMOND light source, Unite Kingdom) for the discussion on the CST modeling of the superconducting cavity. This research was supported by the Converging Research Center Program through the Ministry of Science, ICT and Future Planning, Korea (NRF-2014M3C1A8048817).

[1]S. Shin, S. Kwon, D.-T. Kim, D.-E. Kim, M. Kim, S.-H. Kim, S.-C. Kim, J. Kim, C. Kim, B. Park, S.-S. Park, S.-J. Park, E. Park, Y. Son, J. Yoon, B. Lee, E. Lee, J.-W. Lee, H.-S. Lee, Y. Joo, J. Choi, T. Ha, W. Hwang, I. Hwang, J.-Y. Lee, B. Oh, C.-H. Lee, H.-S. Lee, J.-Y. Kim, J. Y. Hwang, S. H. Nam, and M. Cho, J. Instrum. **8**, P01019 (2013).
[2]I. Hwang, J. Huang, M. Kim, B. Lee, C. Kim, J. Choi, M. Him, H. Lee, D. Moon, E. Lee, S. Nam, S. Shin, and M. Cho, Rev. Sci. Instrum. **85**, 055113 (2014).
[3]S. An, Y. Joo, and H. Kang, J. Korean Phys. Soc. **56**, 2024–2028 (2010).
[4]Y. Sohn, Y. Joo, I. Yu, I. Park, M. Chun, H. Park, T. Ha, H. Kim, C. Park, H. Huang, and S. Nam, in *Proceedings of the International Particle Accelerator Conference* (Shanghai, China, May 20–25, 2013), pp. 2390–2392.
[5]A. Piwinski, DESY-98-179 (1998).
[6]*CST Microwave Studio User's Manual*, available on website http://www.hep.ph.ic.ac.uk/uknfic/fets/docs/mws/Getting%20Started.pdf.
[7]Y. Saito, N. Matuda, S. Anami, A. Kinbara, G. Horikoshi, and J. Tanaka, IEEE Trans. Electr. Insul. **24**, 1029–1032 (1989).
[8]J. Lokiewicz, T. Fadina, J. Kula, A. Bilinski, and Z. Yu, in *Proceedings of the 11th Workshop on RF Superconductivity* (Lübeck, Travemünder, Germany, 2003), ThP31.
[9]S. K. Esin, T. N. Habibullin, L. V. Kravchuk, V. V. Peplov, V. A. Puntus, and G. V. Romanov, in *2nd European Particle Accelerator Conference* (Nice, France, 12–16 Jun, 1990), pp. 506–507.